

Electrochemical Evaluation of Carbon Steel and Galvanized Steel Rebar Embedded in Sustainable Ternary Blended Concrete by EIS

Aldo Emelio Landa-Gomez¹, Gerardo Fajardo-San Miguel², Dulce Maria Anahi Cruz-Moreno², Andres Carmona-Hernandez³, Ricardo Orozco-Cruz³, Ricardo Galván-Martínez^{3*}

¹Facultad de Ingeniería Civil, Universidad Veracruzana, Xalapa, Veracruz, México.

²Universidad Autónoma de Nuevo León, Facultad de Ingeniería Civil, UANL-FIC, Ciudad Universitaria, San Nicolás de los Garza, N.L. México.

³Unidad Anticorrosión, Instituto de Ingeniería, Universidad Veracruzana, Boca del Río, Veracruz, México.

*Corresponding author: Ricardo Galván-Martínez, email: rigalvan@uv.mx; phone: +52 229 112 9203.

Received December 13th, 2023; Accepted June 6th, 2024.

DOI: <http://dx.doi.org/10.29356/jmcs.v69i2.2178>

Abstract. This research investigated the effect of supplementary cementitious materials (SCMs) on the electrochemical corrosion behavior of carbon steel (CS) and galvanized steel (GS) rebars embedded in ternary blended systems by electrochemical impedance spectroscopy (EIS) measurements. These steel-concrete systems were prepared with a water/cement ratio of 0.45 and partial substitutions of the Ordinary Portland Cement (OPC) by sugarcane bagasse ash (SCBA) and fly ash (FA). The OPC and SCMs were characterized by scanning electronic microscopy (SEM) and X-ray diffraction (XRD) analysis. The EIS results indicated that the SCMs contributed to the electrochemical behavior of ternary steel-concrete at an early stage of the hydration process. The higher values of resistance (R_{film}) were obtained in the concentration of 30 % substitution. This fact was attributed to the oxygen decrease on the metal surface, which was confirmed by the decrease of the electrochemical double layer capacitance (C_{dl}) value with respect to the reference specimen.

Keywords: Corrosion; impedance; ternary concrete; pozzolan; durability.

Resumen. Esta investigación estudió el efecto de materiales cementantes suplementarios (SCM) sobre el comportamiento de la corrosión electroquímica de barras de refuerzo de acero al carbono y acero galvanizado embebidas en sistemas de concreto ternarios mediante mediciones de Espectroscopía de Impedancia Electroquímica (EIS). Estos sistemas acero-concreto se prepararon con una relación agua/cemento de 0.45 y sustituciones parciales del Cemento Portland Ordinario (OPC) por ceniza de bagazo de caña (SCBA) y cenizas volantes (FA). El OPC y los SCM se caracterizaron mediante análisis de microscopía electrónica de barrido (SEM) y difracción de rayos X (DRX). Los resultados del EIS indicaron que los SCM contribuyeron al comportamiento electroquímico del acero-hormigón ternario en una etapa temprana del proceso de hidratación. Los mayores valores de resistencia (R_{film}) se obtuvieron en la concentración del 30 % de sustitución. Este hecho se atribuyó a la disminución de oxígeno en la superficie del metal, lo que fue confirmado por la disminución del valor de capacitancia electroquímica de doble capa (C_{dl}) con respecto a la muestra de referencia.

Palabras clave: Corrosión; impedancia; hormigón ternario; puzolana; durabilidad.

Introduction

SCMs are used as a corrosion prevention method for reinforced concrete structures (RCS), because they offer a satisfactory solution by increasing durability [1]. They also contribute by reducing environmental problems related to the generation and final disposal of industrial or agro-industrial materials [2]. In addition, the cement manufacturing process requires a high energy demand and generates carbon dioxide (CO₂) emissions into the atmosphere [3].

Previous research has reported that SCMs contain amorphous silica in its chemical composition, and when they are used in Portland cement-based materials, they react chemically with calcium hydroxide [Ca(OH)₂] to form new hydration products. This interaction occurs at later ages where the cementitious matrix microstructure is improved, thus increasing its mechanical and durability properties [4,5].

Nowadays, the SCBA and FA have been studied as a part of the ecological concrete. The SCBA is an agro-industrial waste material that has acceptable physicochemical properties that allow it to be used as a natural pozzolan [6,7]. On the other hand, FA is a sub-product of coal combustion in thermal power plants, which is captured by electrostatic precipitators from the flue gas before being released to the outside [8].

SCBA and FA have been studied as composite concretes, i.e., concretes made with OPC and two SCMs, thus obtaining ternary concretes. Ríos Parada et al. [9] studied the effects of the addition of SCBA and FA in ternary concretes. Their main finding was that the pozzolanic reaction of untreated sugarcane bagasse ash (UtSCBA) is beneficial at later ages, because the mix with 60 % CPC, 20 % FA and 20 % SCBA decreased the strength at early ages, but after 90 days, this strength was similar to the control specimen.

Likewise, Franco-Lujan et al [1] evaluated the corrosion of reinforced ternary concretes containing FA and UtSCBA by monitoring corrosion potentials (E_{corr}) and Linear Polarization Resistance (LPR) techniques. In a period of the exposure time of 2,500 days, they found that the ternary concretes containing 10 % and 20 % UtSCBA decreased the chloride ions diffusion, which they attributed to the changes in the cementitious matrices caused by the pozzolanic reactions of UtSCBA.

Franco Lujan et al. [10] evaluated the capability of ternary concretes with UtSCBA and FA versus free and total chlorides retention, they observed that long-term exposure of ternary concretes did not lead to Ca(OH)₂ dissolution and decalcification of calcium silicate hydrate (CSH). The principal conclusion in this research is focused on the fact that the ternary concretes in combinations of 20 % FA+10 % UtSCBA and 20 % FA + 20 % UtSCBA increased chloride retention by approximately 12.12 % and 12.74 % compared to control concrete.

According to the above studies, the use of SCBA and FA combinations are satisfactory, however, the corrosion phenomena in ternary steel-concrete systems should be further evaluated to prevent premature deterioration of the RCS.

Due to the need to know in detail the corrosion processes of steel-concrete systems, the EIS technique has been applied to characterize the microstructure of the concrete, the interfacial properties of the cement-based materials, as well as the corrosion parameters, using an equivalent electrical circuit (EEC) model [11]. EIS technique consists of applying an alternating potential signal of small amplitude (10-20 mV) to the steel embedded in the concrete, in a selected frequency range. This sinusoidal perturbation of potential (ΔE) must be imposed under steady-state conditions, and the electrode response is a sinusoidal current (ΔI) with a phase difference (Φ) of the applied signal. Therefore, the impedance, represented by Z , measures the relationship between ΔE and ΔI [12,13].

To obtain the electrochemical parameters with EIS, Vedalakshmi et al. [14] established an alternative method to predict the chloride diffusion coefficient (D) in steel-concrete systems using the Warburg diffusion coefficient (D_{w}) which was determined from EIS. Oliveira and Cascudo [15] evaluated the effects of pozzolanic mineral additions to concrete under chloride attack using EIS and LPR and electrical resistivity techniques. Using the EIS technique, they showed the changes in impedance values at the steel-concrete interface under study. Likewise, Zheng et al. [16] applied the EIS technique to evaluate the influence of calcium ion in the concrete pore solution on the passivation of galvanized steel bars.

Recently, Rezende et al [17] evaluated the Sugarcane bagasse ash sand (SBAS) as an additive in reinforced concrete. Unlike the SCBA, SBAS is a heavy ash collected at the bottom of the boilers with quartz composition. They conducted an electrochemical investigation of SBAS using EIS and E_{corr} measurements in Ca(OH)₂ and NaCl 3.5 %. They reported that during the curing process (Ca(OH)₂), SBAS concrete formed a passivation film after a longer time (7–14 days) than the reference (REF) (7 days), and the passive film showed higher resistance values than the REF sample. After 191 days in the chloride medium, REF and SBAS samples

presented similar corrosion resistance. On the other hand, Annaba et al [18] assessed the benefits of incorporating higher natural volcanic pozzolan (NMP) content (ranging from 10 % to 50 % by weight) as a cement substitute in mortar and concrete mixtures on compressive strength and corrosion resistance of reinforced concrete when exposed to 3 % NaCl solution after 3 and 90 days. The authors found that the highest compressive and bending strengths were observed in mixes with 30 % of NMP. EIS and E_{corr} results indicated that the addition of natural pozzolan enhanced the corrosion resistance of reinforced concrete exposed to chloride attack.

Therefore, the aim of the present work was elucidating the contribution of SCMs in the microstructure of a ternary concrete and their influence on the electrochemical behavior of carbon steel (CS) and galvanized steel (GS) steel rebars, analyzing the initial passivity. According to these facts, the SCMs were characterized by SEM, energy dispersive X-ray spectroscopy (EDS) and XRD. The ternary steel-concrete systems were electrochemically characterized by EIS and E_{corr} measurements. The LPR technique was developed at the initial period of the exposure time and at 90 days.

Experimental

Preparation of ternary concrete systems

The ternary concretes were made with stone aggregates with a nominal maximum size of 12 mm and 4.75 mm, respectively. The aggregates met ASTM C33/C33M designation specifications. SCBA was obtained from Veracruz, Mexico, and pulverized with a ball mill to a size of less than 75 μm . The FA was acquired from coal-fired power plant located Coahuila, Mexico. Both materials met ASTM C618 specifications, and were classified as class N and F pozzolans, respectively. Likewise, OPC was used, which complied with the ASTM C150 standard specifications. Partial substitution of Portland cement in 10, 20 and 30 % by SCMs were carried out, these percentages correspond to 50 % of SCBA and 50 % of FA. Table 1 shows the identification of the ready-mixed concrete.

Table 1. Identification of the concrete.

Nomenclature	Description
REF	Reference concrete
10SF	90 % OPC – 05 % SCBA - 05 % FA
20SF	80 % OPC – 10 % SCBA – 10 % FA
30SF	70 % OPC – 15 % SCBA – 55 % FA

On the other hand, current water was used as mixing water and a high-range liquid water-reducing additive, which complied with ASTM C1602/C1602M and C494/C494M, respectively. The concrete mixtures were designed according to the American Concrete Institute procedure in section 211.1. The method used to provide the concrete mixes was the absolute volumes method. Table 2 shows the materials proportion for a volume of 0.4 m^3 .

Table 2. Concrete mixture proportions.

Concrete	Cement (kg)	Water (kg)	Sand (kg)	Gravel (kg)	SCBA (kg)	FA (kg)	Additive (kg)
REF	192.00	91.80	298.50	344.00	0.00	0.00	0.32
10SF	172.80	91.80	293.50	344.00	9.60	9.60	0.32
20SF	153.60	91.80	288.50	344.00	19.20	19.20	0.32
30SF	134.40	91.80	283.50	344.00	28.80	28.80	0.32

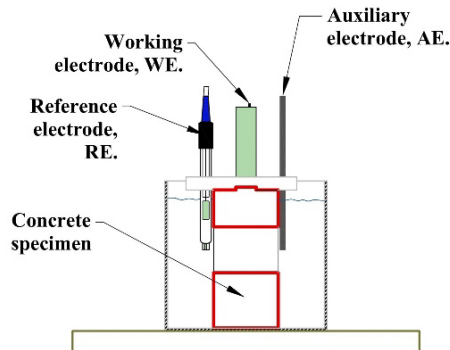


Fig. 2. Schematic representation of the electrochemical cell.

Surface characterization

SEM analyses were carried out on a scanning electron microscope on powder samples, to know the morphology of the OPC and SCMs. The EDS technique was also applied to analyze the elemental chemical composition of the materials, which were coated with gold/palladium before the analysis. XRD analyses were performed using an X-ray diffractometer with $\text{CuK}\alpha$ radiation. XRD patterns were recorded in the 2θ range of 10 to 60° . The XRD patterns were analyzed using the High Score Plus software to identify the crystalline phases.

Results and discussion

SEM/EDS analysis of SCMs

The ternary concretes were made with stone aggregates with a nominal maximum size of 12 mm and 4.75 mm, respectively. The aggregates met ASTM C33/C33M designation specifications Fig. 3(a) shows the micrograph of the OPC, irregular angular and prismatic particles with different sizes were observed. This morphology was attributed to the clinker pulverization process [22].

As shown in Fig. 3(b), the morphology of SCBA consisted of prismatic particles with different sizes. These particles are angular and elongated, as well as agglomerations of fine particles smaller than $10\ \mu\text{m}$.

The micrograph of the FA (Fig. 3(c)) showed spherical and prismatic particles with different sizes. It was identified that spherical particles were mostly solid, however, hollow spherical particles were also observed, known as cenospheres. Also, sphere-shaped particles filled with other particles of the same shape, but of smaller size, known as plerospheres. Arenas-Piedrahita et al. [8] associated this morphology to the mineral impurities combustion in the coal, which upon melting form a suspension that is extracted outside the kiln, and these solidifies in a form of glassy spherical particles.

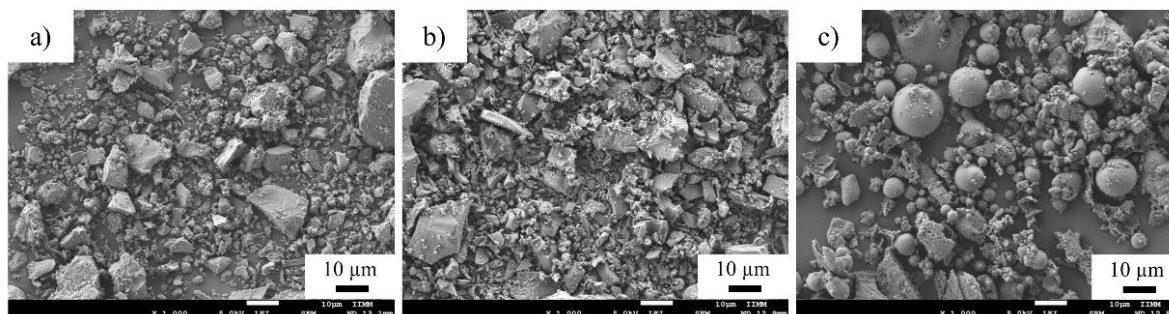


Fig. 3. SEM images at a magnification of 1,000x: (a) OPC, (b) SCBA and (c) FA.

The results of EDS mapping on the OPC and SCMs samples are shown in Fig. 4 and Table 3. The OPC analysis (Fig. 4(a)) showed a homogeneous distribution of mainly Ca (34.29 wt. %) and Si (4.25 wt. %). Cruz Moreno et al., [23] reported that the chemical composition of OPC obtained by X-Ray Fluorescence (XRF) is mainly constituted of calcium oxide (CaO) and silicon dioxide (SiO₂) as obtained in this research.

Table 3. Chemical composition determined by EDS mapping of OPC and SCMs.

Element (wt. %)	O	Si	Al	Fe	Ca	K	S	Mg	C	Ti	Na	P
OPC	56.57	4.25	0.64	1.91	34.29	1.08	0.98	0.02	0.26	-	-	-
SCBA	58.23	17.34	2.73	3.68	2.67	4.08	-	1.96	-	0.36	8.26	0.69
FA	69.29	14.45	7.74	2.90	2.26	0.96	0.31	0.16	1.20	0.73	-	-

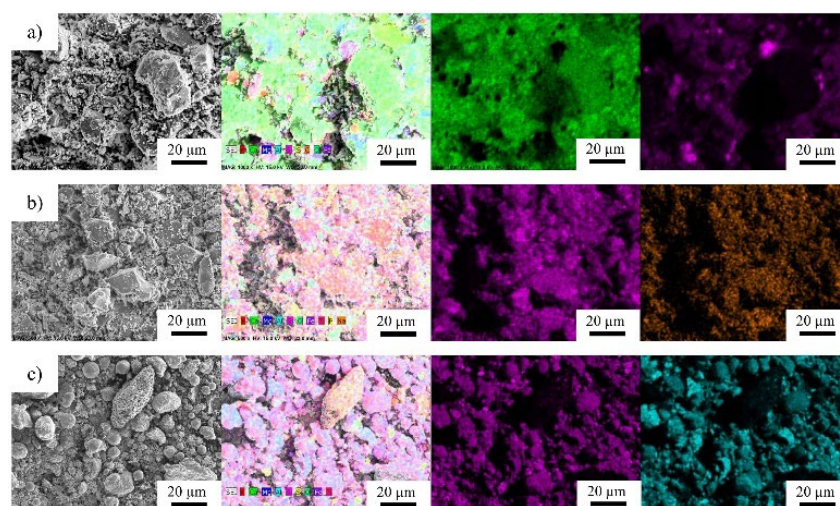


Fig. 4. Elemental distribution obtained from EDS mapping: (a) OPC, (b) SCBA and (c) FA.

In Fig. 4(b), the elemental distribution of SCBA indicated the presence of Si (17.34 wt. %) and Na (8.26 wt. %). The prismatic particles contain Si and O, while Na alkalis are present in the conglomerate particles. The elements obtained have been reported in oxides previously by Ríos-Parada et al. [9], where silicon dioxide represented more than 60 % of the sample.

On the other hand, EDS results showed that the FA particles contained Si (14.45 wt. %) and Al (7.74 wt. %) as shown in Fig. 3(c). It is important to point out that the Si is concentrated in the prismatic particles and Al in the plerospheres. Moreover, it was observed the presence of carbon, which can be related with the combustion process rate and temperature, as well as to the nature and type grinding of the carbon before calcination [7]. These findings agree with those reported by Wang et al. [24].

It is important to mention that SCBA and FA contain high concentration of Si, Al and Fe, and are potentially pozzolanic materials, it is to say, they are chemically reactive with Ca(OH)₂. [8,25] Therefore, they can be classified as type N and F pozzolans, respectively, according with the specifications of ASTM C618 standard.

XRD analysis of SCMs

Fig. 5(a) shows the XRD diffractogram of OPC, which characteristic peaks corresponding to the crystalline phases of dicalcium silicate (C2S) and tricalcium silicate (C3S). Secondary peaks were also identified as: tricalcium aluminate (C3A), tetracalcium ferroaluminate (C4FA), calcium monoxide (CaO), and gypsum. The crystalline phases

corresponding to the four main chemical compounds of the OPC analyzed by Marchon & Flatt [26], which were related to the chemical analysis obtained with EDS. The C3S and C2S in the hydration process produced primary calcium silicate gel hydrate and $\text{Ca}(\text{OH})_2$ crystal, which developed the mechanical properties of the concrete [27,28].

In Fig. 5(b), the XRD pattern of the SCBA showed a semi-crystalline material, because it has containing amorphous (vitreous) material. This fact is because an amorphous halo is observed in the 2θ region from 14 to 35° . Furthermore, characteristic quartz ($\alpha\text{-SiO}_2$) and cristobalite ($\beta\text{-SiO}_2$) peaks were detected. Secondary peaks of magnetite (Fe_3O_4), dialuminium trioxide (Al_2O_3) and other compounds were also identified. The $\beta\text{-SiO}_2$ phase was associated with the high calcination temperatures produced in the cauldrons, while the crystalline $\alpha\text{-SiO}_2$ phase was attributed to the presence of adhered sand during sugarcane harvesting [29]. Fig. 5(c) shows the XRD pattern of FA, where a peak corresponding to quartz ($\alpha\text{-SiO}_2$) and secondary peaks like hematite (Fe_2O_3) and mullite ($\text{Al}_6\text{Si}_2\text{O}_{13}$) were identified. These phases were responsible for the delay in pozzolanic reactivity because they are inert, and the glassy phase reacted at later ages. The FA exhibited an amorphous halo between 2θ angles from 17 to 37° , which is characteristic of vitreous silicoaluminates materials [9].

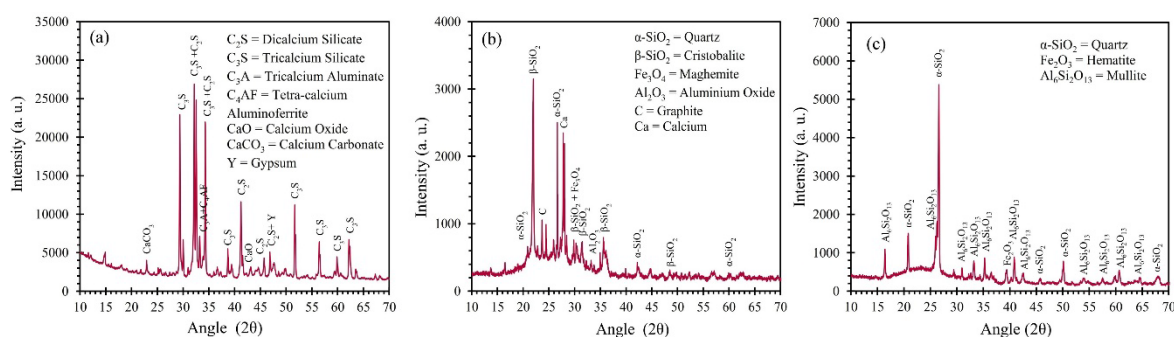


Fig. 5. XRD patterns: (a) OPC, (b) SCBA and (c) FA.

Corrosion potential (E_{corr}) and corrosion current density (i_{corr})

Fig. 6 shows the i_{corr} , and E_{corr} results of the CS and GS embedded in the concretes tested. The interpretation of the results was as follows: in the case of i_{corr} , four zones were delimited with dashed horizontal lines as proposed by Andrade & Alonso [30], whereas the E_{corr} results were delimited with a continuous vertical line with two zones, low and high corrosion probability (-270 mV vs SCE) according to the ASTM C876 standard.

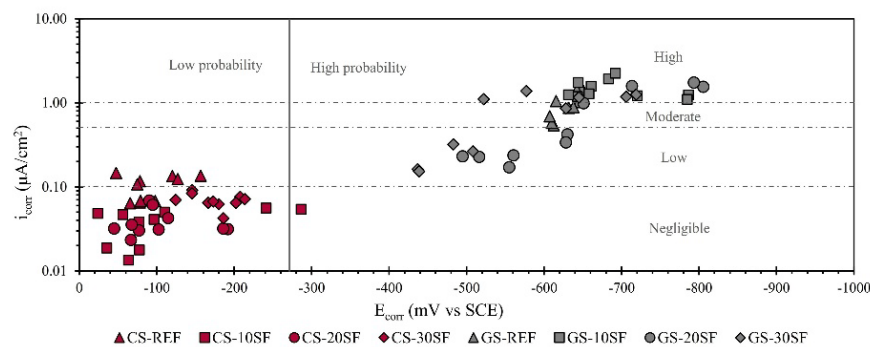


Fig. 6. i_{corr} vs E_{corr} values of the CS y SG steels during 90 days of exposure.

The E_{corr} results showed that the potential in the different concretes got values lower than -270 mV indicating that the reinforcing steel bar had low corrosion probability. The i_{corr} values showed that the CS embedded in the different concretes were localized in zones corresponding to low and negligible corrosion level. Castro-Borges et al. [31] attributed this electrochemical behavior to the initial passivation of the steel due

to the formation of the passive layer. Some i_{corr} values of the CS embedded in REF concrete were found in the range from 0.1 to 0.5 $\mu\text{A}/\text{cm}^2$ indicating a passive behavior, however, with the addition of SCMs, the i_{corr} decreased to values less than 0.1 $\mu\text{A}/\text{cm}^2$ in CS embedded in 10SF, 20SF, and 30SF. This behavior was associated with the low oxygen diffusion in concrete due to the complexity of the cementitious matrix because of the pore-filling effect produced by the SCMs [1].

On the other hand, the E_{corr} values of GS embedded in REF and 10SF concretes shown an active behavior because the values were found in range of -600 to -784 mV; as the concentration of SCMs increased, the E_{corr} values corresponding to GS in 20SF and 30SF got values less than -600 mV, indicating a passive process. The behavior obtaining by the E_{corr} values are agree with the behavior of i_{corr} values.

The GS embedded in REF and 10SF concretes got i_{corr} values corresponding to a moderate and high corrosion level. Padilla & Alfantazi [32] attributed this active behavior to the zinc dissolution, leading to the zincate ion formation $[\text{Zn}(\text{OH})_4]^{2-}$ until these ions can saturate the solution and then precipitate as zinc oxide (ZnO) or zinc hydroxide ($\text{Zn}(\text{OH})_2$). On the other hand, the i_{corr} of GS in 20SF and 30SF concretes showed values corresponding to a low corrosion level. Tan et al. [33] attributed this behavior to a zinc passivation process in alkaline medium with the presence of $\text{Ca}(\text{OH})_2$.

EIS measurements

Fig. 7 shows the EIS results of CS and GS steels embedded in the ternary concretes at the age of 28 and 90 days. The impedance (Z) values at high frequencies were related to the first time constant (τ_1) attributed to the concrete resistance. At the mid-frequencies, Z values were related with the second time constant (τ_2) and it were associated with the concrete microstructure and the steel-concrete interface. Likewise, this τ_2 involved the corrosion products layer plus the precipitation of $\text{Ca}(\text{OH})_2$ on metal surface during the hydration process. Finally, the Z values at low frequencies were related to the third time constant (τ_3). It was attributed to the corrosion resistance of the steel rebars, that is, the charge transfer resistance of the corrosion process. Finally, the Warburg impedance was associated with the diffusion process of the electroactive species [12].

Fig. 7(a) and 7(c) show the EIS spectra of the CS. All Nyquist curves shown that the corrosion was controlled by a mass transfer (diffusion) process with a typical Warburg behavior at low frequencies because they showed a slope with 45° approximately at lower frequencies. Oliveira & Cascudo [15] attributed this behavior to oxygen diffusion that controlled the electrochemical process. At low frequencies, the EIS spectra of the CS embedded in REF concrete showed a decrease in the real impedance (Z') magnitude with respect to the CS in the 10SF, 20SF and 30SF concretes at both age. This behavior was related to the reduction of the diffusion species (like as oxygen) to the metal surface, provoking that the corresponding oxygen reduction reaction in the electrochemical corrosion was limited [34].

Fig. 7(b) and 7(d) show the EIS spectra of GS. Like CS rebars. Nyquist curves revealed that the corrosion was controlled by a mass transfer process (diffusion), present a typical Warburg behavior. Zheng et al. [35] attributed this behavior to the soluble reactants transport from the solution to the electrode/electrolyte interface, which indicated that the corrosion process was controlled by the cathodic reaction. It is important to point out that at the age of 28 days, the EIS spectra of the GS embedded in the ternary concretes with 0 to 20 % of SCMs presented similar values of impedance, however, a further addition of the SCMs (30 %) and a higher age of exposure (90 days) led to an increase of impedance values. This behavior is attributed to the filling effect that the SCMs generated in the concrete microstructure [16].

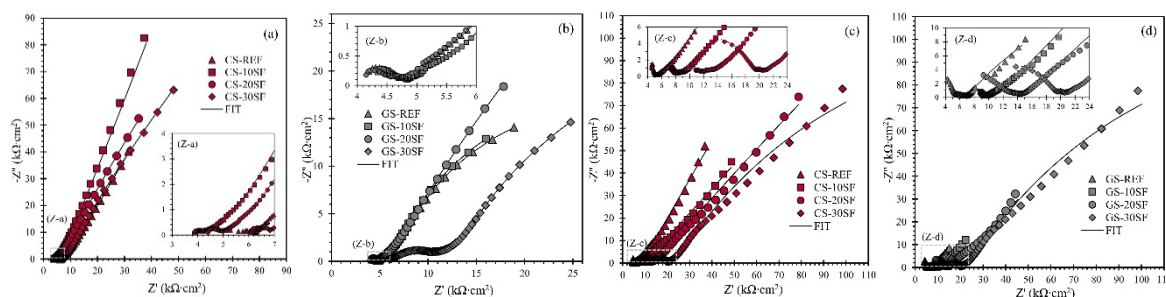


Fig. 7. Nyquist diagrams of the steels embedded in the ternary concretes (a) CS 28 days, (b) GS 28 days, (c) CS 90 days and (d) GS 90 days.

The fitting of the EIS spectra was carried out with the equivalent electrical circuit (EEC) shown in Fig. 8(a), which has been proposed previously by other authors [34,35]. The electrochemical parameters with the physical meaning of the EEC (Fig. 8(b)) include the solution resistance (R_s), the constant phase element (CPE_c) that simulated the non-ideal concrete capacitance (C_c), the concrete resistance (R_c), CPE_{film} that simulated the non-ideal capacitance (C_{film}) of the steel-concrete interface or film adsorbed in the metal surface, the resistance of the steel-concrete interface (R_{film}), CPE_{dl} that simulated the C_{dl} , the charge transfer resistance (R_{ct}) and the semi-infinite Warburg element (W). The time constants τ_2 (C_{film} - R_{film}) and τ_3 (R_c - C_c) are in series and in parallel with respect to τ_1 (C_{dl} - R_{ct}). The C_{dl} value was calculated using the Brug's et al equation [36]. The Warburg impedance coefficient (σ_w) was determined with the equation proposed by Vedalakshmi et al. [14], which was used as an indicator to quantify the diffusion resistance of electroactive species.

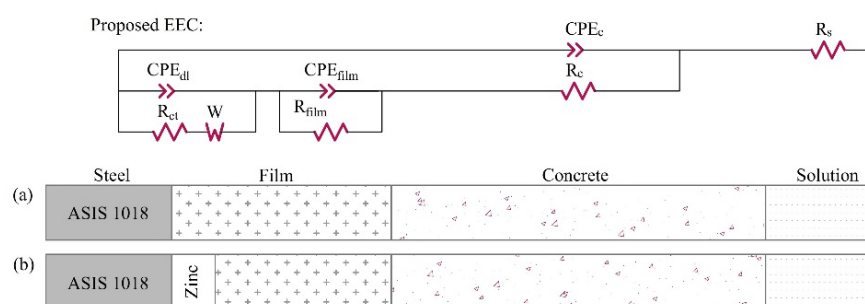


Fig. 8. EEC proposed for fitting EIS spectra, (a) concrete system of CS and (b) concrete system of GS.

Table 4 shows the results of the electrochemical parameter derived from the fitting of EIS spectra at the age of 90 days, using the proposed EEC of Fig. 8(a). From this Table, it can be seen that the R_c increased as the SCMs concentration increased. This behavior was attributed to the pozzolanic reactions between the SiO_2 of the SCMs and $Ca(OH)_2$, which generated a secondary calcium silicate hydrate (CSHS) gel. This secondary product filled the existing pores in the interfacial transition zone (ITZ) inside the cementitious matrix, contributing to the densification of the concrete internal microstructure [9]. The 10SF, 20SF and 30SF systems presented an increment of 27 %, 44 % and 126 % respectively, with respect to R_c value of REF.

Table 4. Parameters obtained from the EEC adjustment of the EIS spectra of CS and GS at the age of 90 days.

Nomenclature	R_c	C_c	R_{film}	C_{film}	R_{ct}	C_{dl}	σ_w	Chi-squared
	($k\Omega \cdot cm^2$)	($\mu F/cm^2$)	($k\Omega \cdot cm^2$)	($\mu F/cm^2$)	($k\Omega \cdot cm^2$)	($\mu F/cm^2$)	($\Omega m^2 \cdot s^{-1/2}$)	
CS-REF	4.80	1.15E-04	8.45	4.71E+02	159.30	4.43E+02	2.28E-02	1.69E-04
CS-10SF	6.45	3.91E-05	9.25	4.02E+02	162.30	4.41E+02	3.27E-02	3.80E-04
CS-20SF	7.23	2.50E-05	10.35	1.51E+02	180.50	2.15E+02	5.57E-02	7.00E-04
CS-30SF	11.96	7.17E-05	13.41	8.55E+01	321.30	2.00E+02	7.62E-02	2.59E-04
GS-REF	5.32	1.76E-04	1.30	1.11E-01	1.71	1.24E+03	2.38E-02	6.80E-04
GS-10SF	6.42	1.16E-04	3.56	3.97E+01	4.20	1.16E+03	4.55E-02	2.09E-04
GS-20SF	7.32	1.66E-06	6.87	1.29E-04	5.80	1.12E+03	5.53E-02	6.52E-04
GS-30SF	10.96	9.13E-05	7.30	2.57E-02	10.53	1.05E+03	6.05E-02	5.09E-04

According to Table 4, the electrochemical behavior of the CS concrete systems was as follows: the R_{film} increased by 9, 22 and 59 % for the CS at 10SF, 20SF and 30SF, with respect to REF. Sohail et al. [34], attributed this increment due to the precipitation of $\text{Ca}(\text{OH})_2$ on steel surface during the corrosion process. On the other hand, the R_{ct} values increased due to the improvement of R_{film} and R_{c} , where the R_{ct} of the CS embedded in 10SF, 20SF, and 30SF incremented by 2, 13 and 102 %, respectively with respect to the R_{ct} of the CS in REF, which is attributable to the physical properties of the concrete microstructure, as well as to the chemical properties of the pore solution [15]. Likewise, the C_{dl} of CS embedded in 10SF, 20SF and 30SF decreased by 1, 51, and 55 % respectively, with respect to the C_{dl} of CS in REF. This behavior indicates the decrease of electrical charge on the capacitor. Vedalakshmi & Palaniswamy [37] considered that the capacitance value depends on the species adsorbed, such as chlorides, oxygen, and hydroxides on metal surface. In addition, they proposed that C_{dl} values below $500 \mu\text{F}/\text{cm}^2$ are considered for a passive state of the reinforcing steel and $1,000 \mu\text{F}/\text{cm}^2$ to an active state. According to the C_{dl} values, the CS was found in a passive state, which was agreed to the results obtained by i_{corr} . The passive behavior was related with the increase of σ_{w} values as the concentration of SCMs increased in the cementitious matrix. The behavior of σ_{w} value suggested that the concentration of electroactive species on metal surface decreased.

On the other hand, in GS-concrete systems were found a similar behavior to CS-concrete systems. The values of GS R_{film} in 10SF, 20SF and 30SF incremented by 174, 428 and 462 %, respectively with respect to REF. Zheng et al.[16] attributed the increase in R_{film} values of galvanized steel to the presence of $\text{Ca}(\text{OH})_2$ which generated the reaction between $\text{Zn}(\text{OH})_4^{2-}$ ion to $\text{Ca}(\text{OH})_2$ to produce calcium hydroxyzincate (CHZ), generating the process of passivation of Zn. The R_{ct} values also increased as the proportion of SCMs in the concrete mixture was higher. The increase of R_{ct} was agreed with the decrease of C_{dl} values, which is related to the decrease of the kinetic of corrosion process as the electrical charge accumulated decreased in the electrochemical double layer. Whilst the σ_{w} increased by 91, 132, and 154 % in 10SF, 20SF, and 30SF respectively, versus REF. This behavior of σ_{w} can support the decrease of electroactive species on metal surface and provoke the decrease in C_{dl} values.

Influence of SCM on the corrosion process

The corrosion study showed that the reinforcing steels (CS-GS) embedded in ternary concretes made with SCM, presented better performance against corrosion during the initial stage of the hydration process by increasing the electrochemical parameters values such as R_{c} , R_{film} , R_{ct} and σ_{w} . The physical meaning for this behavior was attributed to the contribution of the SCMs in the microstructure of the concrete. When SCBA and FA particles were found inside the cementitious matrix, pozzolanic reactivity started at the age of 60 days when SiO_2 molecules adsorbed the existing $\text{Ca}(\text{OH})_2$ crystal [4]. In some studies [1,9], this interaction has been identified, however, the mechanism of the pozzolanic reaction has not been reported. Therefore, this research proposes the following reaction between SiO_2 molecules with $\text{Ca}(\text{OH})_2$ expressed as oxides:



The hydration product obtained is CSHS gel, which improved the concrete microstructure, generating the increase in R_{c} . This behavior was associated with the increment in the amorphous SiO_2 concentration within the cementitious matrix, leading to the generation of CSHS and thus increased pore nucleation. Fig. 9(a) and 9(b) show a scheme with the pores filling present in the concrete microstructure due to the generation of CSHS.

It is important to point out that the improvement of the microstructure of the concretes contributed directly to the electrochemical behavior of the steels for the CS-concrete systems (Fig. 9(a)), the differences observed in this system were attributed to the passive film (corrosion products film) formed on the steel bars. According to literature [38,39] the passive film is composed by a thin internal layer of magnetite, which is an insoluble mixed oxides such as iron oxide II (FeO) and iron oxide III (Fe_2O_3); and an external layer of iron oxide III (maghemite). The corrosion mechanism occurs in the local pore solution, in presence of oxygen according to the following reactions [40].

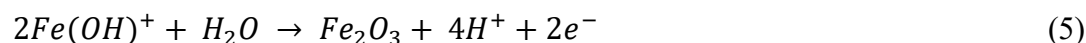
Cathodic reaction:



Anodic reaction:



The formation of iron hydroxide ions $Fe(OH)^+$ is directly dependent on the concentration of OH^- ions present in the cementitious matrix. As the pH increased, the adsorption of $Fe(OH)^+$ ions also increased, which caused that the E_{corr} shifted to nobler values, provoking that the $Fe(OH)^+$ ions oxidize to ferric oxide (III) according to the following reaction:



According to the ferric oxide (III) formation, the increase of the R_{film} of CS in ternary concretes was attributed to the high concentration of OH^- ions produced by the oxygen cathodic reaction and those present in the cementitious matrix in the first 28 days because the concrete microstructure was more porous. As the exposure time increased, a more protective passive film was generated by the higher concentration of Fe_2O_3 according to the reaction (5). After this fact, the pore nucleation after 60 days, the passive film becomes stable, because the oxygen diffusion through the concrete microstructure is limited by the passive film. This behavior is corroborated by the increase in σ_w and R_{ct} values and the decrease in C_{dl} .

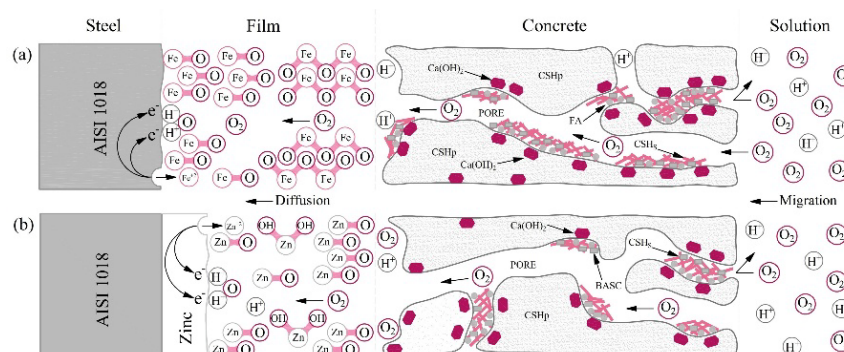
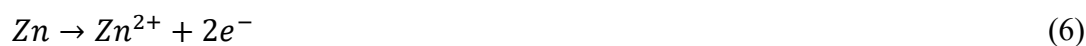
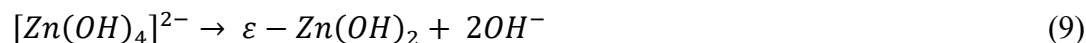


Fig. 9. Physical explanation scheme of the corrosion process, a) CS - concrete and b) GS – concrete systems.

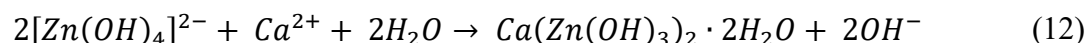
Fig. 9(b) shows the schematic representation of the GS-concrete corrosion system. This system presents the same concrete microstructure as the CS-concrete systems discussed previously. In this system, the R_{film} is an important factor for the electrochemical behavior of the steel bar, which was attributed to the improvement of the concrete microstructure. Several studies have reported the corrosion and passivation mechanisms of zinc in alkaline media. Tittarelli & Bellezze [41] reported that the zinc corrosion process is carried out with the dissolution of zinc generating a $Zn(OH)_4^{2-}$ ion. Likewise, dissolution continues of this ion to supersaturate the solution until it precipitates as ZnO or $Zn(OH)_2$. Pokorny et al. [42] reported that this corrosion products film is not able to protect the metallic surface and he described the corrosion mechanism at pH 11.5 to 12.2, being the cathodic reaction the oxygen reduction (2), while the Zn dissolution (anodic reaction) takes place according to the following reactions [42]:



The $Zn(OH)_4^{2-}$ ions saturated the solution and precipitated as ZnO and $(Zn(OH)_2)$ according to the following reactions:



Where the ε is the zinc hydroxide phase. Tan & Hansson [33] reported that zinc passivity is originated when the $Zn(OH)_4^{2-}$ ion reacts with the $Ca(OH)_2$ in a pH range of 12.5 to 13.3, and the CHZ [$Ca(Zn(OH)_3)_2$] is produced by the following reaction:



According to the R_{film} behavior, the GS embedded in the REF and 10SF concretes got a low value, due to the dissolution of the zinc, which was in active state, generating the increase of i_{corr} the E_{corr} shifted to more electronegative potential values. On the other hand, the increase of the R_{film} of GS embedded in 20SF and 30SF concretes was attributed to the formation of a passive film, which is supported by the CHZ production. The R_{film} behavior was also corroborated by the increment of the R_{ct} and the decrease of the C_{dl} . This behavior was attributed to the decrease of oxygen diffusion through the passive film and concrete microstructure. As shown in Fig. 9(b), it should be noted that the σ_w value increased mainly due to the closed or almost closed pores diameter.

Conclusions

The influence of SCMs on the electrochemical behavior of CS and GS rebars embedded in ternary concrete mixtures was investigated by EIS. The following conclusions can be drawn:

- For bulleted lists The EIS results revealed that a further addition of SCMs in concrete (30 SF) improved the microstructure of the cementitious matrix and provoked the increment of R_c in a 126 % at the age of 90 days compared to those obtained in the reference sample (REF). The behavior showed was attributed to the generation of SCHS.
- The cementitious matrix with SCMs contributed to a passive film formation on surface of both (CS and GS) steel bars. This film promoted the initial passivity process in these systems. The R_{film} increased 59 and 462 % to CS and CG respectively.
- A higher concentration of SCMs in the cementitious matrix limited the oxygen diffusion process from the environment to reinforcement bar surface. This behavior was corroborated with the increase of σ_w value by 235 and 154 % for CS and CG, respectively.
- R_{ct} values were associated with the presence of a passive film that induced the decrement of C_{dl} to 55 and 16 % by CS and GS respectively. This behavior was associated to lower amount of water into the concrete because the filling effect of pores produced by pozzolanic reactions of SCBA and FA.
- Finally, it is possible to say that the partial substitution of OPC by SCMs (SCBA -FA) promoted the improvement of the concrete microstructure and the initial CS and GS steels passivity. Therefore, it can be considered as an alternative to increase the service life of RCS.

Acknowledgements

The authors express their gratitude to National Council for Science and Technology (CONACYT), the SECIHTI-Mexico for the financing granted to projects CB-2016/285453 and IT-301307, the Research Laboratory and Innovation in Building Materials of the Civil Engineering Faculty of Autonomous University of Nuevo León and the Doctorate Program of Materials and Nanoscience of MICRONA Center of Veracruzana University, for the financial and technical support to A.E. Landa-Gomez for the realization of this research.

References

1. Franco-Luján, V. A.; Maldonado-García, M. A.; Mendoza-Rangel, J. M.; Montes-García, P. *Constr. Build. Mater.* **2019**, *198*, 608–618. DOI: <https://doi.org/10.1016/j.conbuildmat.2018.12.004>.
2. Sales, A.; Lima, S. A. *Waste Manage.* **2010**, *30*, 1114–1122. DOI: <https://doi.org/10.1016/j.wasman.2010.01.026>.
3. Scrivener, K. L.; John, V. M.; Gartner, E. M. *Cem. Concr. Res.* **2018**, *114*, 2–26. DOI: <https://doi.org/10.1016/j.cemconres.2018.03.015>.
4. Paris, J. M.; Roessler, J.G.; Ferraro, C. C.; DeFord, H. D.; Townsend, T. G. *J. Clean. Prod.* **2016**, *121*, 1–18. DOI: <https://doi.org/10.1016/j.jclepro.2016.02.013>.
5. Lin, Y.; Alengaram, U.J.; Ibrahim, Z. *J. Build. Eng.* **2023**, *78*, 107500. DOI: <https://doi.org/10.1016/j.jobe.2023.107500>.
6. Cordeiro, G.C.; Tavares, L.M.; Toledo-Filho, R. D. *Cem. Concr. Res.* **2016**, *89*, 269–275. DOI: <https://doi.org/10.1016/j.cemconres.2016.08.020>.
7. Khalil, M. J.; Aslam, M; Ahmad, S *Constr. Build. Mater.* **2021**, *270*, 121371. DOI: <https://doi.org/10.1016/j.conbuildmat.2020.121371>.
8. Arenas-Piedrahita, J. C.; Montes García, P.; Mendoza-Rangel, J.M.; López-Calvo, H. Z.; Valdez-Tamez, P. L; Martínez-Reyes, J. *Constr. Build. Mater.* **2016**, *105*, 69–81. DOI: <https://doi.org/10.1016/j.conbuildmat.2015.12.047>.
9. Ríos-Parada, V.; Jiménez-Quero V.G.; Valdez-Tamez, P.L.; Montes-García, P. *Constr. Build. Mater.* **2017**, *157*, 83–95. DOI: <https://doi.org/10.1016/j.conbuildmat.2017.09.060>.
10. Franco-Luján, V. A.; Mendoza-Rangel, J. M.; Jiménez-Quero V. G.; Montes-García, P. *Cem. Concr. Compos.* **2021**, *120*, 104040. DOI: <https://doi.org/10.1016/j.cemconcomp.2021.104040>.
11. Hu, X.; Shi, C.; Liu, X.; Zhang, J.; de Schutter, G. *Cem. Concr. Compos.* **2019**, *100*, 1–14. DOI: <https://doi.org/10.1016/j.cemconcomp.2019.03.018>.
12. Ribeiro, D. V.; Abrantes, J.C.C. *Constr. Build. Mater.* **2016**, *111*, 98–104. DOI: <https://doi.org/10.1016/j.conbuildmat.2016.02.047>.
13. Lazanas, A.C.; Prodromidis M.I. *ACS Meas. Sci. Au.* **2023**, *3*, 162–193. DOI: <https://doi.org/10.1021/acsmeasuresciau.2c00070>.
14. Vedalakshmi, R.; Saraswathy, V.; Song, H. W.; Palaniswamy, N. *Corros. Sci.* **2009**, *51*, 1299–307. DOI: <https://doi.org/10.1016/j.corsci.2009.03.017>.
15. Oliveira AM de, Cascudo O. *Constr. Build. Mater.* **2018**, *192*, 467–477. DOI: <https://doi.org/10.1016/j.conbuildmat.2018.10.100>.
16. Zheng, H.; Dai, J, G.; Poon, C. S.; Li, W. *Cem. Concr. Res.* **2018**, *108*, 46–58. DOI: <https://doi.org/10.1016/j.cemconres.2018.03.001>.
17. de A.M., Rezende M; Corradini, P.G.; Sales, A; Mascaro, L.H. *Constr. Build. Mater.* **2023**, *397*, 132341. DOI: <https://doi.org/10.1016/j.conbuildmat.2023.132341>.
18. Annaba, K; El Mendili, Y.; Stout, H.; Ech-chebab, A.; Ouaki, B.; Cherkaoui, M.; et al. *Case Stud. Constr. Mat.* **2023**, *19*, e02620. DOI: <https://doi.org/10.1016/j.cscm.2023.e02620>.
19. Stern, M.; Geary, A. L. *J. Electrochem. Soc.* **1957**, *104*, 56. DOI: <https://doi.org/10.1149/1.2428496>.
20. Hu, J.; Deng, P.; Li, X.; Zhang, J.; Wang, G. *Constr. Build. Mater.* **2018**, *183*, 180–188. DOI: <https://doi.org/10.1016/j.conbuildmat.2018.06.015>.
21. Rivera-Corral, J. O.; Fajardo, G.; Arluguie G.; Orozco-Cruz, R.; Deby, F., Valdez, P. *Constr. Build. Mater.* **2017**, *147*, 815–826. DOI: <https://doi.org/10.1016/j.conbuildmat.2017.04.186>.
22. Chakraborty, S.; Jo, B. W.; Yoon, Y. S. in: *Smart Nanoconcretes and Cement-Based Materials*, Elsevier, Netherlands, **2020**, 183–213 DOI: <https://doi.org/10.1016/B978-0-12-817854-6.00007-6>.
23. Cruz-Moreno, D.; Fajardo, G.; Flores-Vivian, I.; Orozco-Cruz, R.; Ramos-Rivera, C. *Appl. Surf. Sci.* **2020**, *531*, 147355. DOI: <https://doi.org/10.1016/j.apsusc.2020.147355>.
24. Wang, W.; Lu, C.; Li, Y.; Yuan, G.; Li, Q. *Constr. Build. Mater.* **2017**, *138*, 486–495. DOI: <https://doi.org/10.1016/j.conbuildmat.2017.02.039>.

25. Cordeiro, G. C.; Tavares L. M.; Toledo Filho, R.D. *Cem. Concr. Res.* **2016**, 89, 269–275. DOI: <https://doi.org/10.1016/j.cemconres.2016.08.020>.
26. Marchon, D.; Flatt, R. J. in: *Science and Technology of Concrete Admixtures*, Elsevier, **2016**, 129–145 DOI: <https://doi.org/10.1016/B978-0-08-100693-1.00008-4>.
27. Van Damme, H.; Pellenq, R. J. M.; Ulm, F.J. in: *Developments in Clay Science*, Elsevier, Vol. 5, **2013**, 801–817 DOI: <https://doi.org/10.1016/B978-0-08-098258-8.00027-4>.
28. Charan, S.S.; Dey, S.; Kumar, V.V.P.; Sireesha, T. *Architecture, Structures and Construction.* **2023**, 3, 347–372. DOI: <https://doi.org/10.1007/s44150-023-00096-7>.
29. Cordeiro, G. C.; Toledo Filho, R. D.; Tavares, L. M.; Fairbairn, E. de M. R. *Cem. Concr. Res.* **2009**, 39, 110–115 DOI: <https://doi.org/10.1016/j.cemconres.2008.11.005>.
30. Andrade, C.; Alonso, C. *Constr. Build. Mater.* **1996**, 10, 315–328. DOI: [https://doi.org/10.1016/0950-0618\(95\)00044-5](https://doi.org/10.1016/0950-0618(95)00044-5).
31. Castro-Borges, P.; Balancán-Zapata, M.; Zozaya-Ortiz, A. *Adv. Mater. Sci. Eng.* **2017**, 1–8. DOI: <https://doi.org/10.1155/2017/6973605>.
32. Padilla, V.; Alfantazi, A. *Constr. Build. Mater.* **2014**, 66, 447–457. DOI: <https://doi.org/10.1016/j.conbuildmat.2014.05.053>.
33. Tan, Z. Q.; Hansson, C. M. *Corros. Sci.* **2008**, 50, 2512–2522. DOI: <https://doi.org/10.1016/j.corsci.2008.06.035>.
34. Sohail, M.G.; Kahraman, R.; Alnuaimi, N.A.; Gencturk, B.; Alnahhal, W.; Dawood, M.; et al. *Constr. Build. Mater.* **2020**, 232, 117205. DOI: <https://doi.org/10.1016/j.conbuildmat.2019.117205>.
35. Zheng, H.; Dai, J. G.; Li, W.; Poon, C. S. *Constr. Build. Mater.* **2018**, 166, 572–580. DOI: <https://doi.org/10.1016/j.conbuildmat.2018.01.174>.
36. Brug, G. J.; van den Eeden, A. L. G.; Sluyters-Rehbach M.; Sluyters, J. H. J. *Electroanal. Chem. Interf. Electrochem.* **1984**, 176, 275–295. DOI: [https://doi.org/10.1016/S0022-0728\(84\)80324-1](https://doi.org/10.1016/S0022-0728(84)80324-1).
37. Vedalakshmi, R.; Palaniswamy, N. *Mag. Concr. Res.* **2010**, 62, 177–189. DOI: <https://doi.org/10.1680/mac.2010.62.3.177>.
38. Ahmad, Z. in: *Principles of Corrosion Engineering and Corrosion Control*, Elsevier, **2006**, 609–646. DOI: <https://doi.org/10.1016/B978-075065924-6/50013-1>.
39. Sánchez-Moreno, M.; Takenouti, H.; García-Jareño, J. J.; Vicente, F.; Alonso, C. *Electrochim. Acta.* **2009**, 54, 7222–7226. DOI: <https://doi.org/10.1016/j.electacta.2009.07.013>.
40. Popov, B. N. in: *Corrosion Engineering*, Elsevier, **2015**, 525–556 DOI: <https://doi.org/10.1016/B978-0-444-62722-3.00012-4>.
41. Tittarelli, F.; Bellezze, T. *Corros. Sci.* **2010**, 52, 978–983. DOI: <https://doi.org/10.1016/j.corsci.2009.11.021>.
42. Pokorný P.; Tej, P.; Kouřil, M. *Constr. Build. Mater.* **2017**, 132, 271–289. DOI: <https://doi.org/10.1016/j.conbuildmat.2016.11.096>.